Published in Photonics Technology Letters (IEEE) 7, issue 9, 1022-1024, 1995
which should be used for any reference to this work

Monolithically Integrated DBR Laser, Detector, and Transparent Waveguide Fabricated in a Single Growth Step

D. Hofstetter, H. P. Zappe, J. E. Epler, *Member, IEEE*, and P. Riel

Abstract— **The monolithic integration of a GaAs–AlGaAs distributed Bragg reflector (DBR) laser with a nonabsorbing grating section, a transparent waveguide, and an absorbing photodetector is reported. Transparent and absorbing segments were defined after growth by vacancy-enhanced quantum-well disordering (VED). Laser output power was 5 mW with a threshold current of 22 mA. Detector current was linearly dependent on the laser output power and the emission from the grating side of the laser could be directly coupled into the detector. The conversion efficiency, defined as the ratio between detector current and laser output power, was 0.47 A/W. Using a comparison with as-grown, SiO_2-capped and SrF_2-capped devices, both lasers and detectors were not seen to be adversely affected by the anneal required for the VED.**

I. Introduction

SEMICONDUCTOR integrated optics offers the potential for small optical systems that may be mass produced. Monolithic integration of the laser into a photonic integrated circuit (PIC) reduces coupling losses and enhances robustness. However, a key problem in achieving integration is the definition of absorbing (lasers, detectors) and transparent (waveguides) regions. Numerous approaches, including evanescent coupling between waveguides and absorbing regions (requiring an additional impedance-matching layer and regrowth, respectively) [1], [2], butt coupling between laser and photodetector (needing mirror dry etch technique) [3] or the use of surface-emitting lasers and photodiodes (requiring high-quality dry-etched mirrors) [4], have been developed to address the integration issue.

We present in this letter a technique for the monolithic integration of a distributed Bragg reflector (DBR) laser with transparent waveguide and photodetector, using VED for the definition of the transparent and absorbing regions [5], [6]. The VED process requires no regrowth to define the transparent areas after epitaxial growth and allows a considerably higher conversion efficiency of laser output power into detector current than previous approaches. Although a rapid thermal anneal (RTA) of 960 °C and 24 s is necessary for the process, no degradation in the performance of lasers or photodetectors was noted. We thereby demonstrate the utility of VED for selectively blue-shifting the absorption edge of a single-quantum well double-heterostructure and thus for direct application to PIC fabrication.

The authors are with the Paul Scherrer Institute Zurich, Badenerstrasse 569, 8048 Zurich, Switzerland.

II. Vacancy-Enhanced Quantum-Well Disordering Mechanism

Through a partial disordering of a quantum well (QW) in a double-heterostructure waveguide, the bandgap energy can be increased by up to 60 meV. This results in a blue-shift of the absorption edge and therefore drastically reduces the absorption losses of a waveguide. The disordering is due to interdiffusion of Al and Ga between the GaAs QW and the $Al_{0.3}Ga_{0.7}As$ core region at elevated temperatures, and is greatly increased in the presence of a high concentration of column-III-vacancies. VED relies upon the outdiffusion of Ga ions into a SiO_2 capping layer to generate these vacancies, which diffuse into the heterostructure promoting intermixing. SrF_2 as a dielectric capping material inhibits vacancy generation, such that very little interdiffusion occurs in the regions of the crystal covered by the SrF_2 cap.

By patterning the wafer surface after growth into regions covered by SiO_2 and SrF_2, we are easily able to produce a pattern of transparent and absorbing waveguide sections. The blue-shift due to VED under the SiO_2-cap is temperature and anneal-time dependent, as seen in Table I. A wavelength shift of up to 68 nm under the SiO_2-cap and less than 10 nm under the SrF_2-cap was seen for a 90-s anneal at 960 °C. For the devices described in this letter, we applied only a 24-s anneal in order to minimize p-dopant diffusion into the n-type lower cladding layer. The PL wavelength of the as-grown material used for these experiments was 812 nm, that of the SrF_2-capped material 810 nm, and that of the SiO_2-capped material 793 nm. Fabry–Pérot lasers fabricated from all these types of material showed comparable properties. As-grown material lasers: $\lambda = 827$ nm, $J_{th} = 600$ A/cm^2, $\eta = 0.52$ W/A; SiO_2-capped lasers: $\lambda = 805$ nm, $J_{th} = 500$ A/cm^2, $\eta = 0.42$ W/A; SrF_2-capped lasers: $\lambda = 825$ nm, $J_{th} = 700$ A/cm^2, $\eta = 0.36$ W/A.

III. Fabrication

A metal-organic vapor phase epitaxy (MOVPE) grown layer structure on an n-type Si-doped (10^{18} cm^{-3} Si) GaAs substrate was used for waveguides, photodetectors, and lasers. The layers included an undoped 165-nm-thick $Al_{0.3}Ga_{0.7}As$ core containing a single GaAs quantum well (7 nm), sandwiched between a 1.1-μm-thick $Al_{0.8}Ga_{0.2}As$ lower cladding layer (n-

TABLE I
PHOTOLUMINESCENCE WAVELENGTH SHIFT OF SiO_2-CAPPED AND SrF_2-CAPPED MATERIAL AFTER A RAPID THERMAL ANNEAL OF 30, 60, AND 90 s AND AT DIFFERENT TEMPERATURES

anneal temperature [°C]	wavelength shift SrF_2 [nm]	wavelength shift SiO_2 [nm]
910	0.3 / 1.5 / 3.8	5.1 / 10.9 / 20.5
920	1.6 / 3.4 / 4.9	7.3 / 19.1 / 35.9
930	1.2 / 2.2 / 3.5	10.2 / 24.3 / 40.2
940	2.0 / 4.5 / 8.4	14.4 / 30.2 / 50.6
950	2.6 / 5.9 / 9.3	22.0 / 46.4 / 62.8
960	4.1 / 7.4 / 10.8	28.9 / 48.0 / 68.0

doped 1.5×10^{18} cm^{-3} Si) and a 0.8-μm-thick $Al_{0.8}Ga_{0.2}As$ upper cladding layer (p-doped 10^{18} cm^{-3} Mg). A 100-nm-thick highly p-doped (8×10^{18} cm^{-3} Zn) GaAs cap layer completed the structure.

Processing started with a 200-nm-thick e-beam-evaporated SiO_2 layer, patterned by standard photolithography and reactive ion etching (RIE) using a CF_4 plasma. Without stripping the photoresist, a 250-nm-thick SrF_2 layer was then thermally evaporated. Subsequent lift-off resulted in a nearly planar surface covered completely either with SiO_2 or SrF_2. The samples were then annealed by RTA for 24 s at 960 °C. During anneal, a GaAs proximity cap helps to prevent surface damage of the sample by generating a local As overpressure [7]. Both SrF_2 and SiO_2 were then removed, the former in diluted HCl (HCl/H_2O 1:9, 20 s) and the latter by CF_4 RIE.

Ridge-waveguide DBR lasers were fabricated in this selectively shifted substrate by dry-etching ridge waveguides in a process described previously [8]. The third-order grating had a period of 380 nm, 1:1 mark to space ratio, and a depth of 100 nm. There was a 30-nm buffer layer between grating and waveguide core, giving a coupling coefficient of approximately 100 cm^{-1}. 1200-μm and 1700-μm-long bars were cleaved, yielding two different types of devices: the 1700-μm bars consisted, as shown in Fig. 1, of 500-μm-long pumped sections with 2, 3, and 4-μm ridge widths, 50- to 150-μm-long nonabsorbing DBR grating sections, 500- to 650-μm-long transparent waveguides, and 500-μm-long absorbing photodiodes at the end of the waveguides. We describe in the following only devices with a 150-μm-long grating recess (grating length = 130 μm) and a ridge width of 4 μm. The 1200-μm bars were made out of the former ones by subsequent cleaving of the photodiode and the waveguide, and applying an AR coating after each cleave.

IV. CHARACTERIZATION

The DBR lasers were driven cw at room temperature; maximum output power was 5 mW from the cleaved facet alone, threshold current was 22 mA (J_{th} = 1.1 kA/cm^2), and slope efficiency was on the order of 0.2 W/A. This latter value could be further improved by ensuring a closer wavelength match between the Bragg peak of the grating (814 nm) and the semiconductor gain peak (825 nm). The laser emission from the cleaved facet, as seen in Fig. 2, was single transverse

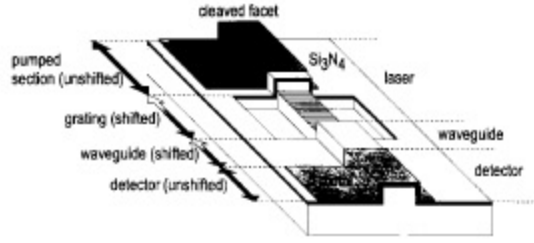

Fig. 1. Schematic diagram of DBR laser monolithically integrated with a transparent waveguide and a photodetector.

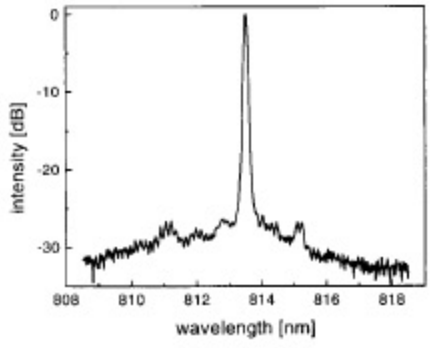

Fig. 2. Optical output spectrum of the DBR laser.

and longitudinal mode with a primary emission peak at λ = 814 m, a sidemode suppression ratio (SMSR) of 25 dB, and a FP mode spacing of 0.155 nm was obtained. The latter value corresponds to a cavity length of 630 μm or an effective grating length of 130 μm. The primary emission peak could be temperature-tuned between 7 and 25 °C without mode hops, leading to a temperature-tuning coefficient of 0.06 nm/°C (Fabry–Pérot lasers: 0.25 nm/°C). Repeated plasma exposure of the contact region during SiO_2-patterning, SiO_2-stripping, and Si_3N_4-contact hole etch increased the series resistance of the lasers drastically (37 W) and resulted in a relatively high threshold voltage, $V(I_{th})$, of 3.3 V.

Due to the moderate grating reflectivity (30–40%) and the relatively high losses in the short transparent waveguide (30 dB/cm), we observed external quantum efficiencies of η = 0.21 W/A from the cleaved facet and η = 0.13 W/A from the AR-coated grating-side facet. This corresponds to a total internal quantum efficiency of 20%. In addition, no significant optical power emitted vertically from the grating was noted. Small ripples are noticeable in the light versus current (L–I) curves from both the cleaved facet and the grating. The presence of these features indicates that the laser is undergoing an optimization of its internal stored energy under changing phase conditions due to carrier- and temperature-induced refractive index changes as current is increased, and are unique features of a laser with one cleaved (nonwavelength selective) and one grating (wavelength selective) reflector. These undulations, which were reproducible and without hysteresis, were less pronounced for emission from the grating side of the laser than from the cleaved facet. This occurs, we believe, because a

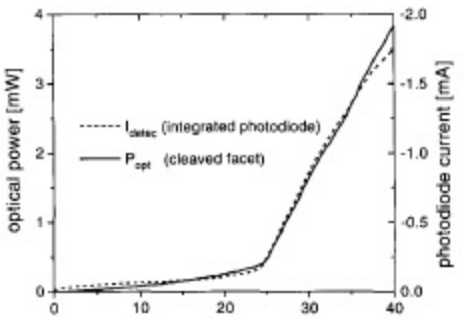

Fig. 3. Optical power and integrated photodetector current versus laser injection current.

decrease in grating reflectivity induces a simultaneous decrease of the laser internal power, resulting in nearly constant laser output power from the grating since the output power is the product of internal power and mirror transmission.

The 1700-μm-long devices added an absorbing 500-μm-long photodetector to these laser/waveguide structures. The resistances parallel to the reverse-biased diodes and between them were all between 3 and 5 kΩ. These small resistances generated large leakage currents across the p-n-junctions and are caused by the incomplete electrical isolation of the remaining upper p-clad between laser and detector. As shown in Fig. 3, we simultaneously measured the cleaved facet output power with an external photodetector and the output power of the grating side with the integrated photodetector. Loss measurements showed that wavelength-shifted waveguides had optical losses comparable to as-grown transparent waveguides and are on the order of 1.5 dB for the short lengths employed. Due to the long absorbing length of the photodiode and based upon the measured small amount of transmitted light (typically 1% of the laser output power), we can assume a high responsivity (>0.6 A/W) of the photodiode; implying >90% quantum efficiency. Conversion of laser output power into detector current was slightly lower (0.47 A/W), if we assume that the laser output from the grating and the cleaved facet are roughly equal. No obvious performance differences between annealed and nonannealed photodetectors was noted.

V. Conclusion

DBR lasers monolithically integrated with a nonabsorbing grating section, a transparent waveguide and an absorbing photodetector have been fabricated while requiring only a single MOVPE growth step. The absorbing and transparent areas on the wafer were defined after growth by VED using two different surface dielectrics, SiO_2 for the transparent regions and SrF_2 for the absorbing segments. The lasers operated cw at room temperature and emitted 5 mW at 814 nm in a single transverse and longitudinal mode. Conversion of laser output power into detector current was typically 0.47 A/W. Device performance is not adversely affected by the VED process, and the simplicity and flexibility of the approach is useful for the design and fabrication of PIC's for numerous applications.

Acknowledgment

The authors gratefully acknowledge the help of M. Moser and H. P. Schweizer for crystal growth, D. Jeggle and A. Vonlanthen for processing assistance, J. Söchtig for enlightening discussions, and M. T. Gale, H. W. Lehmann and R. Dändliker (University of Neuchâtel) for their generous support.

References

[1] R. J. Deri, W. Doldissen, R. J. Hawkins, R. Bhat, J. B. D. Soole, L. M. Schiavone, M. Seto, N. Andreadakis, Y. Silberberg, and M. A. Koza, "Efficient vertical coupling of photodiodes to InGaAsP rib waveguides," *Appl. Phys. Lett.*, vol. 58, pp. 2749–2751, 1991.

[2] K.-Y. Liou, U. Koren, E. C. Burrows, M. Oron, B. J. Miller, M. Young, G. Raybon, and C. A. Burrus, "Operation of integrated InGaAsP/InP optical amplifier-monitoring detector with feedback control circuit," *IEEE Photon. Technol. Lett.*, vol 2, pp. 878–880, 1990.

[3] P. Vettinger, M. K. Benedict, G.-L. Bona, P. Buchmann, E. C. Cahoon, K. Datwyler, H.-P. Dietrich, A. Moser, H. K. Seitz, O. Voegeli, D. J. Webb, and P. Wolf, "Full-wafer technology—A new approach to large-scale laser fabrication and integration," *IEEE J. Quantum Electron.*, vol. 27, pp. 1319–1331, 1991.

[4] C.-H. Chen and S.-C. Lee, "Monolithic integration of an AlGaAs/GaAs surface emitting laser diode and a photodetector," *Appl. Phys. Lett.*, vol. 59, pp. 3592–3594, 1991.

[5] I. Gontijo, T. Krauss, J. H. Marsh, and R. M. De La Rue, "Postgrowth control of GaAs/AlGaAs quantum well shapes by impurity free vacancy diffusion," *IEEE J. Quantum Electron.*, vol. 30, pp. 1189–1195, 1994.

[6] H. P. Zappe, D. Hofstetter and H. E. G. Arnot, "Quantum well engineering for semiconductor integrated optical sensors," *Proc. SPIE*, vol. 2213, pp. 205–212, 1994.

[7] L. J. Guido, N. Holonyak, K. C. Hsieh, R. W. Kaliski, W. E. Plano, R. D. Burnham, R. L. Thornton, J. E. Epler and T. L. Paoli, "Effects of dielectric encapsulation and As overpressure on Al–Ga interdiffusion in $Al_xGa_{1-x}As$/GaAs quantum well heterostructures," *J. Appl. Phys.*, vol. 61, pp. 1372–1379, 1987.

[8] D. Hofstetter, H. P. Zappe, J. E. Epler and J. Schöttig, "Single growth-step GaAs/AlGaAs distributed Bragg reflector lasers with holographically-defined recessed gratings," *IEE Electron. Lett.*, vol. 30, pp. 1858–1859, 1994.